Structure Flexibility Impacts on Robust Active Vibration Isolation Using Mixed Sensitivity Optimisation

Claes Olsson[*][†]

January 15, 2005

Abstract

Active vibration isolation from an arbitrarily, structurally complex receiver is considered with respect to the impacts of structure flexibility on the open- and closed-loop system characteristics. Specifically, the generally weak influence of flexibility on the open-loop transfer function in case of total force feedback, in contrast to acceleration feedback, is investigated.

The open-loop system characteristics are analysed based on open-loop transfer function expressions obtained using modal expansion and on modal model order reduction techniques. To closely demonstrate and illustrate the impacts of flexibility on the closed-loop system performance and stability, a problem of automotive engine vibration isolation from a flexible subframe is presented where the neglected dynamics are represented as an output multiplicative model perturbation.

A physical explanation to why the contribution of flexibility to the open-loop transfer function could be neglected in the case of total force feedback in contrast to acceleration feedback is given. Factors for an individual eigenmode to not significantly contribute to the total force output are presented where the deviation of the mode direction relative to the actuator force direction is pointed out as a key one in addition to modal mass and damping coefficient. In this context, the inherent differences between model order reduction by modal and by balanced truncation are being stressed. For the specific automotive vibration isolation application considered, the degradation of robust performance and stability is shown to be insignificant when obtaining a low order controller by using total force feedback and neglecting flexibility in the design phase.

Keywords

Vibration isolation, structure flexibility, feedback control, $\mathcal{H}_\infty$-control, model reduction

1 Introduction

Considering active vibration isolation of a vibrating machine from a receiver [1] using feedback control and local error sensing, two possible sensor signals are the receiver acceleration and the total force transmitted to the receiver. It has been pointed out that structure flexibility of the receiver will to a greater extent influence the open-loop transfer function in case of acceleration feedback compared to the force one [2,3], with implications on the controller order and closed-loop robustness. Yet, acceleration feedback control has been successfully applied to active vibration isolation [4].

The degree to which modal flexibility couples into the feedback loop is analytically investigated for acceleration, force, and gap feedback signals in [5] and [6]. These studies are carried out in terms of mobilities of receiver, isolation stage, and machine. Where the impact on the open-loop transfer functions is quantified approximately utilising an output multiplicative perturbation model assuming a rigid bodies nominal plant model and one-degree-of-freedom machine and receiver.

While considering isolation of a flexible structure from a disturbance source using sky-hook damping, the differences between feedback controller implementations based on acceleration and force sensing are investigated with respect to closed-loop stability in [7].

In the present study, a general vibration isolation problem is considered covering arbitrarily, structurally complex machines and receivers whereas one-degree-of-freedom isolation and a single feedback sensor are assumed, i.e. single-input single-output (SISO) vibration isolation problems. The objectives

are twofold. Firstly, the impacts of structure flexibility on the open-loop transfer functions from actuator force to total force transmitted to the receiver as well as receiver acceleration are investigated. Furthermore, the absence of flexibility impact on the open-loop transfer function in the case of force feedback is closely examined from a new perspective to give an extended insight into this phenomenon. Secondly, the consequences of neglecting flexibility on closed-loop performance and stability of an automotive vibration isolation application are investigated. Practical issues on weighting functions selections are also discussed when utilising a special formulation of mixed sensitivity optimisation [8].

Section II presents the active vibration isolation application used for illustration throughout the paper. A general analysis of the impacts of structure flexibility on the open-loop transfer function is presented in Section III with associated illustrations. In Section IV, the application specific design specifications are given followed by robust controller design to determine the impacts of flexibility on the closed-loop characteristics. Finally, Section V concludes the paper.

2 The Active Vibration Isolation Application

Figure 1 shows a virtual model of a car engine suspension and a flexibly isolated subframe. The engine is attached to the car body through right- and left-hand side (RHS and LHS) engine mounts, and to *subframe* via a *torque-rod*. The latter is connecting the engine and subframe using the rubber bushings B_1 and B_2 while the four rubber bushings, B_3-B_6, connect the subframe to car body. The engine and subframe suspension system model shown in Fig. 1 has been obtained making use of a multi-body system analysis and simulation software for dynamics [9] where engine and torque-rod are represented as rigid bodies and subframe as a flexible one consisting of six rigid and 24 flexible body modes (using the *Craigh and Bampton* modal synthesis method [10]). This gives a model with 42 physical and modal degrees of fredom (DOF). In the model, the engine mounts and bushings are represented using 6-DOF (three translational and three rotational) spring and damper elements. The two engine mounts and bushing B_1 exhibit non-linear static stiffness characteristics, (for illustration see Figure 2 presenting an example of such non-linear stiffness), and linear damping characteristics, while the bushings B_2-B_6 have linear stiffness and damping characteristics. Taking non-linear properties into account could be crucial to achieve closed-loop stability and acceptable performance when dealing with active engine vibration isolation [11]. However, to simplify the analysis and to clearly discern flexibility impacts from other physical influences, the present study is based on linearised system representations.
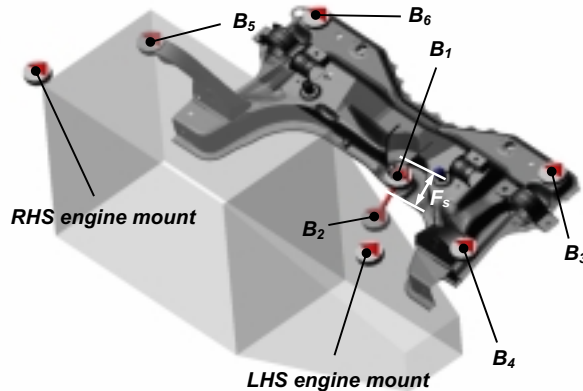

Fig. 1: A model of a car engine and subframe suspension system including rigid body engine and gear box, flexible subframe, rigid body torque-rod, six rubber bushings, and two engine mounts.

The main objective of the torque-rod in this system is to prevent the engine from large angular displacements due to high load engine torque excitation, e.g. corresponding to a rapid acceleration of the car. In conflict with this is the requirement of limiting the forces transmitted from engine to subframe inducing structural vibrations and structure borne noise. Fortunately, these conflicting objectives apply to separate frequency bands, providing potential for successful *active vibration isolation* where the isolation capability could be located to a desired regulation band.

To actively isolate the engine vibrations from subframe, the bushing B_1 connecting torque-rod to subframe is replaced by an actuator consisting of a controllable force in parallel to a *passive stage* with stiffness and damping properties equal to the ones of the removed bushing. This actuator force is applied
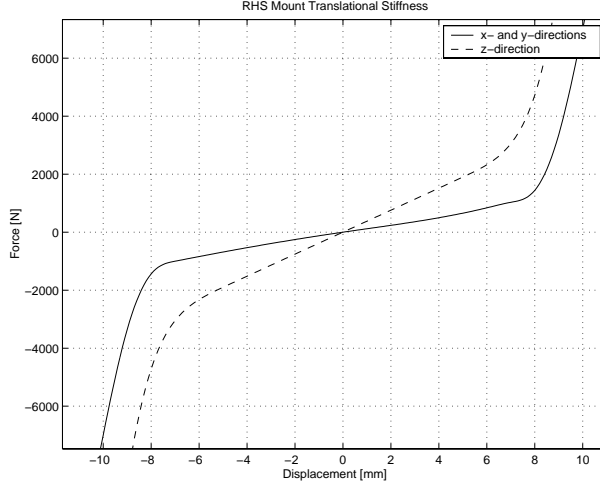
Fig. 2: RHS mount static translational stiffness characteristics, in x-,y-, and z-direction.

in the longitudinal direction of the torque-rod and is indicated F_s in Fig. 1 where the doubled arrowed line symbolises force action and reaction.

When dealing with this SISO active vibration isolation problem using feedback control, a possible feedback signal is the total transmitted force to subframe in the longitudinal direction of the torque-rod, i.e. the sum of the actuator force and the force in the passive stage. Minimising this force to zero means perfect isolation. Another choice of feedback signal is subframe acceleration at the actuator attachment point in the longitudinal direction of the torque-rod. Assuming no other excitation sources than engine excitation, zero acceleration would also correspond to perfect isolation. However, as pointed out in [2,3,5], the choice of sensor signal affects the degree to which flexibility couples into the open loop transfer function. Figure 3 shows the open-loop transfer functions from actuator force output F_s to the two alternative sensor outputs described above, *i.e.* total transmitted force and subframe acceleration, respectively. From the figure, the influence of subframe flexibility is more pronounced in the case of acceleration sensing compared to force one. Comparing the transfer function corresponding to the 42-DOF model to one where the subframe is modelled as a rigid body, the differences in degree of coupling is clear, see Fig. 4.
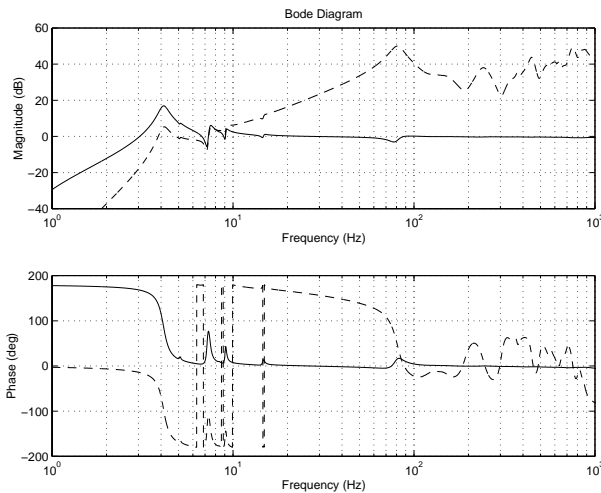

Fig. 3: Transfer functions from F_s (see Fig. 1) to total force transmitted to subframe in the longitudinal direction of the torque-rod (solid), and to subframe acceleration of the actuator attachment point in the direction of the actuator (dashed).
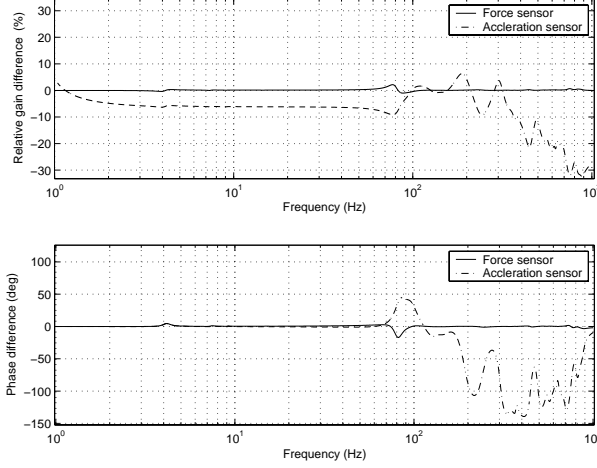
3

Fig. 4: Difference between the open-loop transfer functions when modelling the subframe as a rigid or as a flexible body, for force and acceleration measurements, respectively.

3 Open-loop System Characteristics

In this section, the characteristics of the open-loop transfer functions are investigated. From Fig. 3 it could be seen that in case of total force feedback, the transfer function approaches one for frequencies above approximately 10-20 Hz which plays a key roll in this investigation, see further below.

3.1 Modal Analysis

To study the degree to which flexibility influences the transfer functions from actuator output to total transmitted force and receiver acceleration, respectively, a general linear n-DOF vibration isolation system is considered with equations of motion expressed in terms of a mass matrix $M \in R^{n \times n}$, a damping matrix $C \in R^{n \times n}$, and a stiffness matrix $K \in R^{n \times n}$ as

$$M\ddot{x}(t) + C\dot{x}(t) + Kx(t) = qu(t) \tag{1}$$

where the elements $x(i)(t), i \in \{1,..,n\}$ of $x(t) \in R^n$ typically represent scalar physical displacements. The vector $q \in R^n$ determines the load distribution of the actuator output $u(t) \in R^1$. Considering the application shown in Figure 1, $u(t)$ answers to the actuator force F_s. Equation (1) covers arbitrarily receiver as well as machine dynamics and a 6-DOF passive vibration isolation stage while the actuator is assumed to target one direction only.

Assuming a lightly damped system structure, the response of the system (1) to the actuator excitation could be described using a transfer function as

$$x(i\omega) = H_{xu}(i\omega)u(i\omega) \tag{2}$$

whereas the transfer function $H_{xu}(i\omega)$ is developed using modal expansion [10] according to

$$H_{xu}(i\omega) = \sum_{k=1}^{n} \frac{x_{(k)}^T q x_{(k)}}{\mu_k} \frac{1}{(\omega_{0k}^2 - \omega^2 + 2i\epsilon_k \omega \omega_{0k})} \tag{3}$$

where the eigenmodes $x_{(r)} \in R^n$ and the associated eigenvalues $\omega_{0r} \in R^1$ correspond to the non-trivial solutions to the following equations

$$(K - \omega_{0r}^2 M)x_{(r)} = 0, \quad r \in \{1,..,n\} \tag{4}$$

By analogy with the single degree of freedom system, $\epsilon_r \in R^1$ in Eq. (3) is a modal damping coefficient defined

$$\epsilon_r = \beta_r/(2\omega_{0r}\mu_r) \tag{5}$$

where $\mu_r \in R^1$ and $\beta_r \in R^1$ are the modal mass and modal damping respectively defined as

4

$$\mu_r = x_{(r)}^T M x_{(r)}, \beta_r = x_{(r)}^T C x_{(r)} \tag{6}$$

Remark 1: The light damping assumption is valid when the poles, i.e. eigenvalues when damping is considered, λ_r of the system are well approximated [10] by

$$\lambda_r \approx -\frac{\beta_r}{2\mu_r} \pm i\omega_{0r} \tag{7}$$

The actuator force distribution or alternatively, the actuator stroke direction, is given by q in Eq. (1). If this direction coincides with the direction in which isolation is wanted, the scalar product $-q^T x(t)$ determines the displacement of the passive stage elements in the same direction. Thus, if the stiffness and damping coefficients of the passive stage in the isolation direction are $k \in R^1$ and $c \in R^1$, the total force $y_F(i\omega)$ transmitted to the receiver is given by

$$\begin{aligned} y_F(i\omega) &= u(i\omega) + (k + i\omega c)(-q^T)H_{xu}(i\omega)u(i\omega) \\ &= (1 + H_{1D}(i\omega))\, u(i\omega) \\ &= H_1(i\omega)u(i\omega) \end{aligned} \tag{8}$$

where $H_{1D}(i\omega)$ has the following expression

$$H_{1D}(i\omega) = -(k + i\omega c) \sum_{k=1}^{n} \frac{(x_{(k)}^T q)^2}{\mu_k} \frac{1}{(\omega_{0k}^2 - \omega^2 + 2i\epsilon_k\omega\omega_{0k})} \tag{9}$$

In a similar way, the acceleration of the receiver is given by

$$\begin{aligned} y_a(i\omega) &= -\omega^2 v^T H_{xu}(i\omega)u(i\omega) \\ &= H_2(i\omega)u(i\omega) \end{aligned} \tag{10}$$

where $v \in R^n$ determines the degree of freedom subjected to measurement, i.e. the scalar product $v^T x(t)$ equals the displacement of the measurement point in the direction of sensing.

Comparing $H_1(i\omega)$ and $H_2(i\omega)$ as defined by equations (8) and (10), a key difference is that in addition to n 2nd order modal contribution terms, $H_1(i\omega)$ includes a direct feedthrough term equal to 1 while $H_2(i\omega)$ does not. Consequently, if the transfer function $|H_{1D}(i\omega)|$ in Eq. (9) fulfills $|H_{1D}(i\omega)| << 1$, the transfer function from actuator output to total transmitted force could be approximated by $H_1(i\omega) \approx 1$. This explains the generally less complex appearance of the open-loop transfer function in case of total transmitted force output compared to acceleration one, exemplified by the solid line in Fig. 3. Here and throughout this paper, $|\cdot|$ denotes the absolute value of a scalar variable.

$|H_{1D}(i\omega)|$ in Eq. (9) determines the magnitude of the passive stage force in the direction of the actuator. Thus, physically $H_1(i\omega) \approx 1$ or equivalently $|H_{1D}(i\omega)| << 1$ means that the magnitude of this passive stage force is negligible compared to the magnitude of the actuator force applied in parallel to the passive stage.

3.2 The Total Force Output Case

From the above discussion, it is clear that the passive stage force modal contributions as captured by $H_{1D}(i\omega)$ determine the complexity of the transfer function from actuator force to total transmitted force. This physical insight is formally justified and further explored in this section.

Considering the shape or vibrational pattern of an eigenmode, it could be of rigid body, global flexible, or local flexible character. At a specific frequency, the response of a system could be dominated by rigid body modes, flexible body modes, or combinations of both types. Therefore, when investigating the mechanisms behind the simple appearance of the transfer function from actuator force to total transmitted force, it makes sense to consider general modal contribution in contrast to earlier work [5,6] quantifying model perturbations relative to a nominal model consisting of solely rigid bodies.

Just like in case of the transfer function represented by the solid line in Fig. 3, there could be eigenmodes that contribute significantly to $H_{1D}(i\omega)$ while others could be neglected, possibly independent of the modes' character as pointed out above. Thus, there are partial sums $H_{\Sigma 1}(i\omega)$ and $H_{\Sigma 2}(i\omega)$ of modal terms $h_r(i\omega)$ of $H_{1D}(i\omega)$ where

$$h_r(i\omega) = -(k + i\omega c)\frac{(x_{(r)}^T q)^2}{\mu_r} \frac{1}{(\omega_{0r}^2 - \omega^2 + 2i\epsilon_r\omega\omega_{0r})} \tag{11}$$

such that

$$H_{1D}(i\omega) = H_{\Sigma1}(i\omega) + H_{\Sigma2}(i\omega) \tag{12}$$

which obey the following condition for all frequencies.

$$|H_1(i\omega)| \approx |1 + H_{\Sigma1}(i\omega)| \tag{13}$$

Remark 2: It should be stressed that when considering plant model approximation errors with respect to effects on closed-loop characteristics, they only have to be small over those critical frequency ranges that affect closed-loop stability and performance.

From equations (8) and (12), it follows that for (13) to be true, *i.e.* for the modal partial sum $H_{\Sigma2}(i\omega)$ to insignificantly affect the open loop transfer function, the following condition must hold:

$$|H_{\Sigma2}(i\omega)| << |1 + H_{\Sigma1}(i\omega)| \tag{14}$$

The condition given by Eq. (14) implies that $|H_1(i\omega)| \approx |1 + H_{\Sigma1}(i\omega)|$ but not automatically that $|H_1(i\omega)| \approx 1$. To be able to neglect the eigenmodes included in $H_{\Sigma2}$ and for $|H_1(i\omega)|$ to approximately be unity, $H_{\Sigma1}$ and $H_{\Sigma2}$ must also fulfill the condition given by Eq. (15) in addition to the one given by Eq. (14).

$$|H_{\Sigma1}(i\omega)| = |H_{1D}(i\omega) - H_{\Sigma2}(i\omega)| << 1 \tag{15}$$

Combining (14) and (15), Eq. (16) consequently follows.

$$|H_{\Sigma2}(i\omega)| << 1 \tag{16}$$

The equations (14) and (15) represent principally different situations. When (14) is satisfied alone, the magnitude of the contributions from the modes included in $H_{\Sigma2}(i\omega)$ to the forces in the passive stage is very small compared to the magnitude of the sum of the actuator force and the contributions from the modes included in $H_{\Sigma1}(i\omega)$. In this case, the passive stage force dominates the total transmitted force why the gain of the complete transfer function $H_1(i\omega)$ exceeds one.

On the other hand, for those frequencies where the condition given by Eq. (15) is satisfied in addition to the one given by Eq. (14), it holds that $H_{1D}(i\omega) \approx 0$ which means that the magnitude of the passive stage force is negligible compared to the magnitude of the actuator force.

To determine the contribution from the individual mode r, let $H_{\Sigma1}(i\omega) = \sum_{k \in \{1,..,n\}, k \neq r} h_k(i\omega)$ and $H_{\Sigma2}(i\omega) = h_r(i\omega)$. At $\omega = \omega_{0r}$, the contribution from mode r is maximal. Inserting $\omega = \omega_{0r}$ in Eq. (11) gives

$$|H_{\Sigma2}(i\omega_{0r})| = |h_r(i\omega_{0r})| = \left| \frac{(k + i\omega_{0r}c)(x_{(r)}^T q)^2}{2\mu_r \epsilon_r \omega_{0r}^2} \right| \tag{17}$$

Considering the factors involved in (17), the maximal contribution of mode r is governed by modal mass and modal damping coefficient as defined by Eq. (6), natural frequency ω_{0r}, and passive stage stiffness k and damping c. Moreover, a key reason to whether a mode will have impact on the open-loop transfer function is its direction relative to the actuator force direction. The numerator factor $(x_{(r)}^T q)^2$ in (17) is a scalar product of two real vectors. Thus, if $x_{(r)}$ is orthogonal to q determining the actuator force direction, the contribution of mode r will be zero for all frequencies irrespective of the other factors.

Remark 3: In [5] the impacts of a single receiver mode on the open-loop transfer function is evaluated using an output multiplicative perturbation model where the nominal model is consisting of only rigid bodies. It is stated that the model perturbation will be small if

$$\left| \frac{k\phi_r^2}{2\epsilon_r \omega_{0r}^2} \right| << 1 \tag{18}$$

where ϕ_r is a mass normalised mode shape [5]. The condition (18) does indeed correspond well to the condition given by Eq. (16) with $H_{\Sigma2}(i\omega) = h_r(i\omega)$ evaluated at the natural frequency ω_{0r}. However, the condition (18) does not reveal the importance of the mode directions relative to the actuator force direction which deserves to be stressed. Moreover, the utilisation of an output multiplicative perturbation

model assuming a nominal model consisting of solely rigid bodies certainly leads to illuminating results [5]. But, this might hide the key fact that minor modal contribution is due to low forces in the passive stage compared to the actuator force, and not due to small perturbations from an associated rigid bodies model.

Remark 4: The transfer function $H_1(i\omega)$ in (8) could also be written

$$H_1(i\omega) = 1 + H_{1D}(i\omega) = 1 + n(i\omega)/d(i\omega) = (d(i\omega) + n(i\omega))/d(i\omega)$$

where $n(i\omega)$ and $d(i\omega)$ are two polynomials. If at one of the eigenvalues of the system, i.e. when $\omega = \omega_{0r}$, $|H_{1D}(i\omega)| << 1$, then $|n(i\omega)| << |d(i\omega)|$ and therefore $H_1(i\omega_{0r}) \approx 1$. Thus, minor total modal contribution near any of the eigenfrequencies will appear as an approximate pole/zero cancellation in the associated transfer function from actuator output to total transmitted force. Since, in general, the mode directions and eigenfrequencies are robust to parametric uncertainties, substantial modifications of the system properties are required to change the contribution to the open-loop transfer function of a certain mode from insignificant to significant. Thus, the approximate pole/zero cancellations corresponding to modes with minor contribution to the open-loop transfer function are harmless from a robustness to parametric uncertainty [15] point of view.

3.3 Modal Versus Balanced Model Truncation

The quantification of modal contributions and the conditions given by equations (14) and (15) suggest a way to determine whether a single mode or a sum of several modes could be neglected with little or no impact on the open-loop transfer function. In fact, it constitutes a model order reduction technique based on modal truncation, see *e.g.* [12]. For the considered types of systems, *i.e.* lowly damped mechanical structures, model reduction by modal truncation gives, in general, results similar to the ones obtained by reduction based on balanced truncation. However, there are inherent differences and the methods could give vastly different results for certain system frequency characteristics. In this section, the relation between the two is clarified, and some of the differences are illustrated.

Consider first the following equation of motion corresponding to a general 1-DOF mass-spring system

$$m\ddot{x} + c\dot{x} + kx = u$$

where x is the displacement of the mass and u is a force input applied to the mass. Introducing $q = [\ \dot{x} \quad x\ ]^T$, the system is equivalently represented by

$$\dot{q}(t) = \begin{bmatrix} -c/m & -k/m \\ 1 & 0 \end{bmatrix} q(t) + \begin{bmatrix} 1/m \\ 0 \end{bmatrix} u(t)$$
$$x(t) = \begin{bmatrix} 0 & 1 \end{bmatrix} q(t)$$

(19)

Using similarity transformation, the system could be written on *modal state-space form* [12] as

$$\dot{z}(t) = \begin{bmatrix} -\omega_0\epsilon & \omega_0\sqrt{1-\epsilon^2} \\ -\omega_0\sqrt{1-\epsilon^2} & -\omega_0\epsilon \end{bmatrix} z(t) + \begin{bmatrix} b \\ 0 \end{bmatrix} u(t)$$
$$x(t) = \begin{bmatrix} 0 & c \end{bmatrix} z(t)$$

(20)

for some elements $b \in R^1$ and $c \in R^1$. The undamped natural eigenfrequency ω_0 is $\omega_0 = \sqrt{k/m}$ while the damping coefficient ϵ is $\epsilon = c/(2m\omega_0)$. The corresponding system poles are given by $\lambda = -\omega_0\epsilon \pm \omega_0\sqrt{1-\epsilon^2}$.

Remark 5: The transfer function $H_{1D}(i\omega)$ given by Eq. (9) could be represented on modal state-space form [12] with a block-diagonal A-matrix where the diagonal block Λ_r corresponding to mode r has the following structure:

$$\Lambda_r = \begin{bmatrix} -\omega_{0r}\epsilon_r & \omega_{0r}\sqrt{1-\epsilon_r^2} \\ -\omega_{0r}\sqrt{1-\epsilon_r^2} & -\omega_{0r}\epsilon_r \end{bmatrix}$$

(21)

Evaluating the controllability grammian W_c [13] and the observability grammian W_0 corresponding to Eq. (20) gives

$$W_c = \frac{b^2}{4\omega_0} \begin{bmatrix} \frac{\epsilon^2+1}{\epsilon} & -\sqrt{1-\epsilon^2} \\ -\sqrt{1-\epsilon^2} & \frac{1-\epsilon^2}{\epsilon} \end{bmatrix}$$

(22)

$$W_o = \frac{c^2}{4\omega_0} \begin{bmatrix} \frac{1-\epsilon^2}{\epsilon} & -\sqrt{1-\epsilon^2} \\ -\sqrt{1-\epsilon^2} & \frac{\epsilon^2+1}{\epsilon} \end{bmatrix} \tag{23}$$

which means that the system Hankel singular values (HSVs) [13] $\gamma_i, i = 1, 2$, are

$$\begin{bmatrix} \gamma_1^2 \\ \gamma_2^2 \end{bmatrix} = \frac{b^2 c^2 (1-\epsilon^2)}{16\omega_0^2 \epsilon^2} \begin{bmatrix} 2\epsilon^2 + 1 + 2\epsilon\sqrt{\epsilon^2+1} \\ 2\epsilon^2 + 1 - 2\epsilon\sqrt{\epsilon^2+1} \end{bmatrix} \tag{24}$$

In the above example, the grammians are diagonally dominant when the damping is low. It is also clear that the HSVs corresponding to lowly damped modes approximately appear in pairs. However, since the off-diagonal elements of the controllability and observability grammians in Equations (22) and (23), respectively, are always non-zero (for a mode corresponding to a complex eigenvalue), model order reduction based on modal decoupling could never be identical to the classical one based on diagonalisation of the grammians (*i.e.* balanced reduction).

In general, for the considered types of systems, *i.e.* lowly damped mechanical structures, the modal state-space realisation implies diagonally dominant controllability and observability grammians W_c and W_o. Their structure are given by [12]

$$W_c \approx \mathrm{diag}(w_{ci} I_{2\times 2}), W_o \approx \mathrm{diag}(w_{oi} I_{2\times 2}) \tag{25}$$

for some diagonal elements $w_{ci} \in R^1$ and $w_{oi} \in R^1$ approximately related to the HSVs γ_i as $\gamma_i \approx \gamma_{i+1} \approx \sqrt{w_{ci} w_{oi}}$.

Despite the relation shown above between the grammians corresponding to the two methods, they might give very different results, even for lowly damped mechanical structures. To illustrate such a situation, consider the 2-DOF mass-spring system with the following equations of motion

$$\dot{q}(t) = \begin{bmatrix} -c_1/m_1 & -k_1/m_1 & 0 & 0 \\ 1 & 0 & 0 & 0 \\ 0 & 0 & -c_2/m_2 & -k_2/m_2 \\ 0 & 0 & 1 & 0 \end{bmatrix} q(t) + \begin{bmatrix} 1/m_1 \\ 0 \\ 1/m_2 \\ 0 \end{bmatrix} u(t)$$
$$x(t) = \begin{bmatrix} 0 & 1 & 0 & 1 \end{bmatrix} q(t) \tag{26}$$

with the numerical values given by

$$\begin{bmatrix} m_1 & c_1 & k_1 \\ m_2 & c_1 & k_1 \end{bmatrix} = \begin{bmatrix} 1 & 0.1 & 1 \\ 10 & 0.0315 & 10 \end{bmatrix} \tag{27}$$

The gain of the transfer function is shown as the solid line in Fig. 5. Considering the grammians (28) and (29) of the corresponding modal realisation, they are indeed diagonally dominant in consistence with the 1-DOF example presented above.

$$W_c = \begin{bmatrix} 20.1003 & -1.0013 & -0.0265 & 1.0426 \\ -1.0013 & 20.0000 & -0.3290 & -0.0152 \\ -0.0265 & -0.3290 & 34.9224 & -0.1739 \\ 1.0426 & -0.0152 & -0.1739 & 34.9206 \end{bmatrix} \tag{28}$$

$$W_o = \begin{bmatrix} 2.4937 & -0.1248 & -0.0011 & -0.0236 \\ -0.1248 & 2.5062 & 0.0748 & -0.0019 \\ -0.0011 & 0.0748 & 1.4430 & -0.0072 \\ -0.0236 & -0.0019 & -0.0072 & 1.4430 \end{bmatrix} \tag{29}$$

The HSVs are computed as

$$\begin{bmatrix} \gamma_1 & \gamma_2 & \gamma_3 & \gamma_4 \end{bmatrix} = \begin{bmatrix} 5.2765 & 5.0210 & 5.0088 & 4.7386 \end{bmatrix} \tag{30}$$

To reduce the model given by Eq. (26) to an order of two following the balanced truncation procedure, the states corresponding to the smallest HSVs should be truncated, i.e. those corresponding to γ_3 and γ_4 in Eq. (30). Eliminating these states, a reduced order system with gain represented by the dash-dotted line in Fig. 5 is obtained. The dashed line, in the same Figure, corresponds to the system obtained using modal truncation of the high frequency mode. Clearly, the match between the true system and the reduced order system obtained using balanced truncation is very poor.
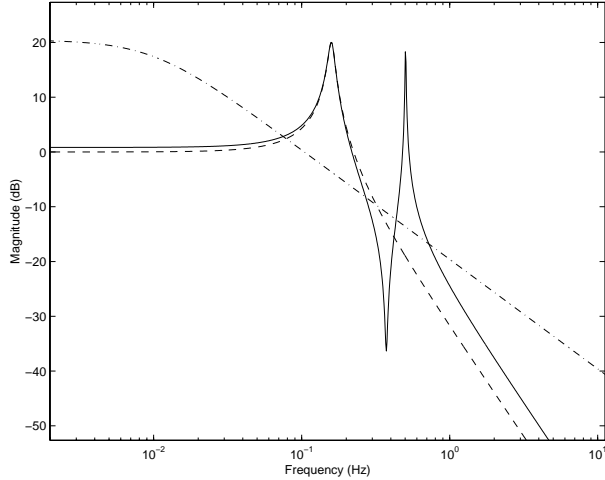
Fig. 5: Gains of the true system given by Eq. (26) (solid), of the system reduced using modal truncation (dashed), and of the system reduced by balanced truncation of the states corresponding to the two smallest HSVs γ_3 and γ_4 in Eq. (30) (dash-dotted).

However, reducing the system by eliminating the states corresponding to γ_2 and γ_3 gives the system represented by the dash-dotted line in Fig. 6, shown together with the gain of the true system and of the system obtained using modal truncation. Although the frequency of the retained mode is slightly shifted, the result is considerably improved.
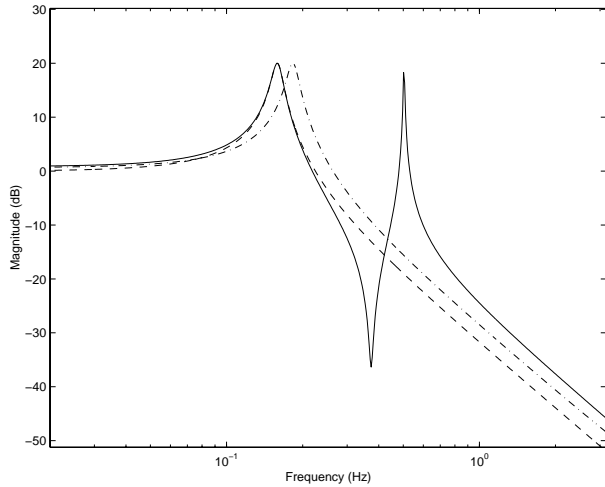

Fig. 6: Gains of the true system given by Eq. (26) (solid), of the system reduced using modal truncation (dashed), and of the system reduced by balanced truncation of the states corresponding to the HSVs γ_2 and γ_3 in Eq. (30) (dash-dotted).

Apparently, there are situations when two adjacent HSVs correspond, approximately, to two different modes. A system which has similar gains at two separate eigenfrequencies, seems to be such a situation. This is a potential pitfall, when using balanced truncation.

With the notation adopted in Section 3.2, the introduced model error due to modal truncation in terms of the additive model perturbation between the nominal plant transfer function $G(i\omega)$ and the reduced rth order one $G_r(i\omega)$ is exactly given by

$$|G(i\omega) - G_r(i\omega)|_\infty = |H_{\Sigma 2}(i\omega)|_\infty \tag{31}$$

since $H_{\Sigma 2}(i\omega)$ equals a transfer function which is a sum of independent modal terms. Throughout the paper, the ∞-sign symbolises $\mathcal{H}_\infty$-norm defined as

9

$$\|F(s)\|_\infty = \sup_{\omega \in R^1} \overline{\sigma}[F(i\omega)] \tag{32}$$

where $\overline{\sigma}(\cdot)$ denotes the largest singular value of a matrix. In case of balanced model reduction, an upper bound on the additive model perturbation exists and is given by [13]

$$|G(i\omega) - G_r(i\omega)|_\infty \le 2(\gamma_{r+1} + \gamma_{r+2} + ... + \gamma_{2n}) \tag{33}$$

As illustrated by the numerical example in the following section, this bound could potentially be very conservative for lowly damped systems.

3.4   Numerical Illustration

The application presented in Section 2 will now be used to illustrate the analysis presented above. At first, the 42-DOF model is linearised [14] about static equilibrium assuming zero excitation which gives an 84th order state space model. Secondly, a modal state-space realisation with a block-diagonal system A-matrix Λ is obtained by state similarity transformation. Thus, the equations of motion are governed by

$$\begin{aligned} \dot{z}(t) &= \Lambda z(t) + Bu(t) \\ y_F(t) &= Cz(t) + u(t) \end{aligned} \tag{34}$$

where the diagonal blocks Λ_r of Λ are either real scalar corresponding to real poles, or 2×2-blocks according to

$$\Lambda_r = \begin{bmatrix} \mathrm{Re}(\lambda_r) & \mathrm{Im}(\lambda_r) \\ -\mathrm{Im}(\lambda_r) & \mathrm{Re}(\lambda_r) \end{bmatrix}$$

corresponding to a complex pole λ_r. From the representation (34) it is possible to obtain transfer functions $h_r^{ss}(i\omega)$ corresponding to the modal terms $h_r(i\omega)$ given by (11). These could be written

$$h_r^{ss}(i\omega) = C_r(sI - \Lambda_r)^{-1}B_r \tag{35}$$

so that the total force output is given by

$$\begin{aligned} y_F(i\omega) &= \left(1 + \sum_{k=1}^{n} h_k^{ss}(i\omega)\right)u(i\omega) \\ &= (1 + H_{1D}^{ss}(i\omega))u(i\omega) \\ &= H_1^{ss}(i\omega) \end{aligned} \tag{36}$$

Denoting the ith elements of the vectors B and C in (34) b_i and c_i, respectively, the vectors B_r and C_r in (35) corresponding to a complex pole are given by $B_r = [\ b_{2r-1}\quad b_{2r}\ ]^T$ and $C_r = [\ c_{2r-1}\quad c_{2r}\ ]$. For a real pole, $C_r = c_r$ and $B_r = b_r$.

   Table 1 in Appendix A presents information about the 43 modes of the linearised engine and subframe suspension system. In addition to the mode character, distinguishing between rigid body, local-, and global-flexible modes, the factors identified as crucial to the degree of modal contribution are given based on the transfer functions (35). In contrast to the expression (11) for $h_r(i\omega)$, $h_r^{ss}(i\omega)$ does not involve the assumption of light damping. Thus, the factors given in Table 1 are approximations of the factors identified using Eq. (17).

   To investigate the modal contributions to the open loop transfer function from actuator force to total force transmitted to the subframe, consider first $|H_{1D}^{ss}(i\omega)|$ as defined by (36) shown as the solid line in Fig. 7. If $|H_{1D}^{ss}(i\omega)| << 1$, it is known from the discussion in Section 3.1 that the passive stage force magnitude will be small compared to the magnitude of the actuator force and thus, that $H_1^{ss}(i\omega) \approx 1$ at these frequencies.

   For the system considered, there are a few rigid body modes corresponding to large displacements of the engine between approximately 4 Hz and 15 Hz, see Table 1. It is likely that these modes will contribute substantially to the open loop transfer function since they evoke large displacement of the passive stage and consequently large passive stage forces. On the other hand, it is not evident what explains the characteristics of $|H_{1D}^{ss}(i\omega)|$ above 15 Hz. From Fig. 7 the total modal contribution corresponding to the modes with natural frequencies above 15 Hz seems to be minor except at frequencies near 80 Hz and 1400 Hz. Investigating the character of the modes [9] reveals that the modes responsible for the dominating modal contribution at these frequencies correspond to rigid body modes characterised by large displacements of the subframe and torque-rod centers of gravity, respectively, see Table 1.
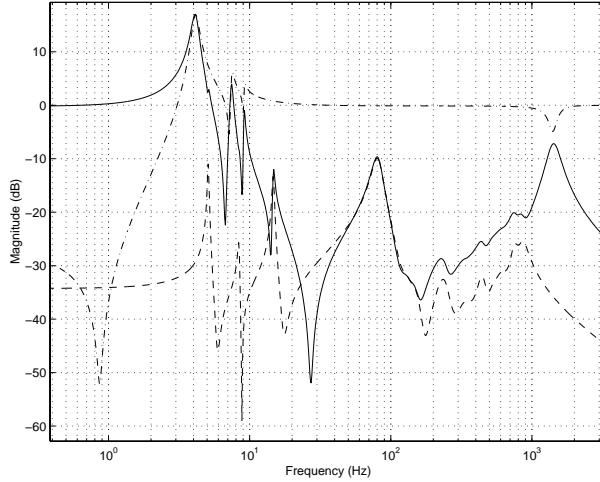
Fig. 7: Magnitudes of three transfer functions; $|H_{1D}^{ss}(i\omega)|$ (solid), $|1+H_{\Sigma 1}(i\omega)|$ as defined by (37) (dashed), and $|H_{\Sigma 2}(i\omega)| = |H_{1D}^{ss}(i\omega) - H_{\Sigma 1}(i\omega)|$ (dash dotted).

In addition to $|H_{1D}^{ss}(i\omega)|$, Fig. 7 also presents $|1+H_{\Sigma 1}(i\omega)|$ and $|H_{\Sigma 2}(i\omega)|$ where $H_{1D}^{ss}(i\omega) = H_{\Sigma 1}(i\omega) + H_{\Sigma 2}(i\omega)$ and $H_{\Sigma 1}(i\omega)$ is defined according to (37).

$$H_{\Sigma 1}(i\omega) = \sum_{k \in \{3,5,7,41\}} h_k^{ss}(i\omega) \tag{37}$$

Applying the conditions (14) and (15) derived in Section 3.2, it is clear that the modes corresponding to $H_{\Sigma 2}(i\omega)$ do not significantly impact the open-loop transfer function. Thus, $H_1^{ss}(i\omega) \approx 1 + H_{\Sigma 1}$. It is worth noticing that $H_{\Sigma 2}(i\omega)$ represents modal contribution dominated by both subframe flexibility as well as rigid body engine, subframe, and torque-rod modes. The limited contribution from the majority of the rigid body modes is due to orthogonality with respect to the actuator direction.

To compare the reduced 8th order model $H_{\Sigma 1}(i\omega)$ obtained above using modal truncation with a corresponding one based on classical model order reduction techniques, an 8th order state-space model $G_D(i\omega)$ has been obtained using balanced model order reduction of the 84th order state-space model $H_{1D}^{ss}(i\omega)$. Fig. 8 presents $|H_{1D}(i\omega)|$, $|H_{\Sigma 1}(i\omega)|$, and $|G_D(i\omega)|$.
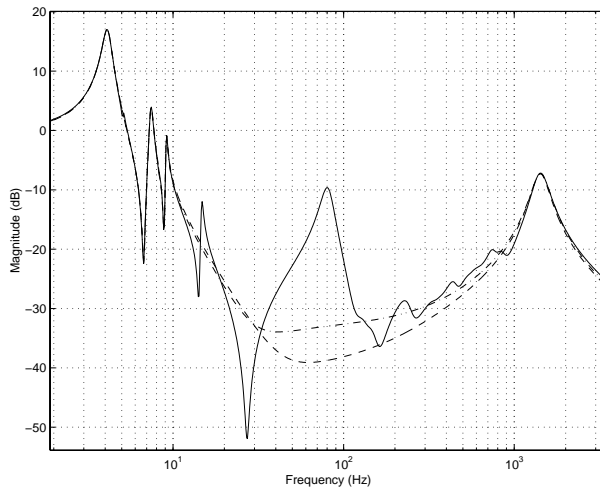

Fig. 8: Magnitudes of three transfer functions; $|H_{1D}(i\omega)|$ (solid), $|H_{\Sigma 1}(i\omega)|$ defined by (37) (dashed), and $|G_D(i\omega)|$ (dash dotted).

In this case, the conformity between $|H_{\Sigma 1}(i\omega)|$ and $|G_D(i\omega)|$ is very high. The degree of model approximation as determined by $|G(i\omega) - G_r(i\omega)|_\infty$ is 0.3098 in case of balanced reduction and 0.3193 when using modal truncation. Since when using the modal representation, $|G(i\omega) - G_r(i\omega)|_\infty = |H_{\Sigma 2}(i\omega)|_\infty$, this norm is bounded from above by

11

$$|G(i\omega) - G_r(i\omega)|_\infty \leq \sum_{k \notin \{3,5,7,41\}} |h_k^{ss}(i\omega)|_\infty \approx 1.323 \qquad (38)$$

Computing the upper bound given by Eq. (33) corresponding to the balanced truncation procedure gives 1.8745. Comparing this bound with the one given by Eq. (38) clearly illustrates its high degree of conservatism when dealing with lowly damped systems.

Studying $|h_{10}^{ss}|$, $|h_{11}^{ss}|$, and $|h_{12}^{ss}|$ shown in Fig. 9, the impact of mode direction relative to the direction of the actuator force on the degree of modal contribution becomes evident. All these modes correspond to rigid body subframe modes determined by its mass and bushings stiffnesses. However, the direction of mode number 12 depicts a rotation of the subframe around the actuator to subframe attachment point, and the displacement of the passive stage in the direction of isolation is thus very small, see Figure 1. Consequently $|x_{(12)}^T q| \approx 0$ which explains Fig. 9.
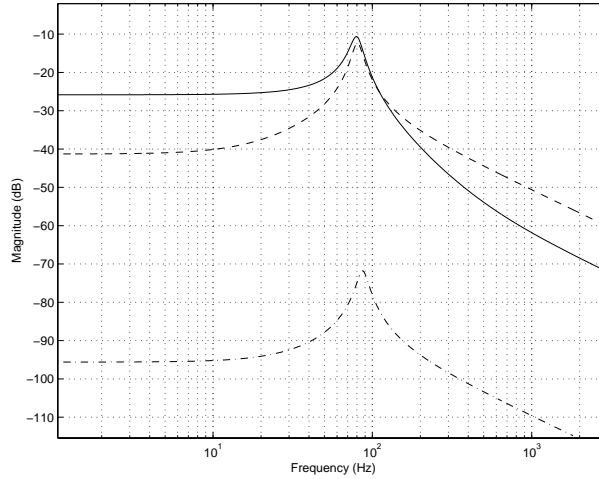

Fig. 9: Magnitudes corresponding to $|h_{10}^{ss}|$ (solid), $|h_{11}^{ss}|$ (dashed), and $|h_{12}^{ss}|$ (dash dotted).

Finally, in light of Remark 3, insignificant modal contribution at frequencies where $|H_{1D}^{ss}(i\omega)|$ is small compared to 1 should appear as approximate pole/zero cancellations. Figure 7 indicates that most poles above 20 Hz will be approximately cancelled by transfer function zeros. This conclusion is confirmed by plotting some of the high frequency poles and zeros of the 84th order model of the engine and subframe suspension system, see Fig. 10. The zeros of the transfer function from actuator force to subframe acceleration would in general obviously not cancel the poles which is also evident from Fig. 10.
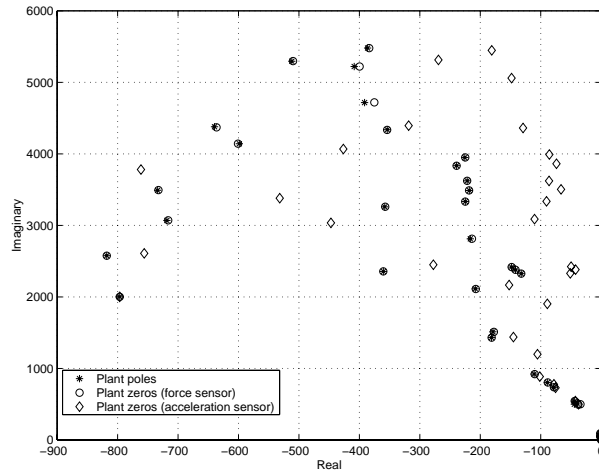

Fig. 10: Some high frequency poles and zeros of the system shown in Fig. 1 corresponding to the two transfer functions presented in Fig. 3, i.e. from actuator force to total transmitted force and receiver acceleration respectively.

4 Closed-loop System Characteristics

The analysis in Sections 3.1 and 3.2, and the illustration presented in Section 3.4 indicate that a large number of modes could potentially be neglected without significantly altering the open-loop transfer function when utilising force feedback. Therefore, force feedback constitutes a better choice compared to acceleration feedback with respect to feedback controller design. Below, the 8th order design model $G(i\omega) = 1 + G_D(i\omega)$ is the one obtained in Section 3.4 based on classical balanced model order reduction.

Taking the characteristics of the engine internal excitation [11] into account, the attenuation of total transmitted force should be approximately -20 dB in the regulation band 30-200 Hz. To minimise the control energy and avoid overloading of the actuator, the controller output, i.e. the force actuator set point, should be as close as possible to zero for frequencies outside the regulation band, i.e. no control action is desired at these frequencies.

4.1 Mixed Sensitivity Optimisation

The design specifications could be expressed in terms of bounds on the sensitivity function $S(s)$ defined as [13]

$$S(s) = (1 + G(s)F(s))^{-1} \tag{39}$$

and on the transfer function $S(s)F(s)$ from output disturbance w to computed plant input u. $F(s)$ is the transfer function of the controller and $G(s)$ is the transfer function of the plant. The following bounds capture the desired closed-loop characteristics

$$
\begin{aligned}
S(s) &= 1, & f &< 30Hz, f > 200\ Hz \\
S(s) &= -20\ \text{dB}, & 30\ Hz &< f < 200\ Hz \\
S(s)F(s) &< -20\ \text{dB}, & f &< 10\ Hz
\end{aligned}
\tag{40}
$$

In addition to the nominal closed-loop requirements as specified by Eq. (40), the controller design shall be carried out with robustness to relative model errors in mind.

From the above closed-loop specifications, application of standard $\mathcal{H}_\infty$ optimisation is one promising way to find a candidate controller $F(s)$. Specifically, the controller design could preferably be formulated as a special mixed sensitivity optimisation problem stated in [8] as

$$\min_{F(s)} \ \left\| \begin{bmatrix} W_1(s)S(s)V(s) \\ W_2(s)S(s)F(s)V(s) \end{bmatrix} \right\|_\infty \tag{41}$$

$W_1(s)$ and $W_2(s)$ in (41) are frequency dependent weighting functions representing the desired closed-loop specifications. The weighting function $V(s)$ provides extra flexibility in shaping the closed-loop characteristics. Denoting $V(s) = M(s)D^{-1}(s)$, any zero of $D(s)$, or alternatively any pole of $V(s)$, coinciding with a pole of $G(s)$ would not be cancelled by $F(s)$ [8,15]. This could be used to avoid pole/zero cancellation of lowly damped modes which is likely to improve robustness to parametric uncertainties.

The minimum damping of the design model poles is approximately 1.4%, see data for mode number 7, Table 1. It is not evident whether cancellation of any of these poles is likely to affect the closed-loop system robustness against parametric uncertainties. However, avoiding cancellation of the two modes with lowest natural frequencies considerably improved the closed-loop characteristics. Cancellation of these poles $p_n, n = \{1, 2\}$, is avoided choosing $V(s)$ as $M(s)D^{-1}(s)$ with

$$D(s) = (s^2 + 2sa_1 + a_1^2 + b_1^2)(s^2 + 2sa_2 + a_2^2 + b_2^2) \tag{42}$$

where $p_n = a_n \pm ib_n$. $M(s)$ could be used to locate some of the closed-loop poles at the zeros of $M(s)$. In this case, $M(s)$ has to be chosen to limit the effect of the two poles of $V(s)$ on the weights on $S(s)$ and $S(s)F(s)$. Therefore, $M(s)$ was chosen as $m_1^{-1}(s)m_2^{-1}(s)$ with $m_n(s)$ equal to a second order notch filter with a peak near the frequencies specified by b_n and with a little higher damping than the one of pole p_n. The inverse of the final weighting functions $W_1(s)V(s)$ and $W_2(s)V(s)$ are shown in Fig. 11 where a small constant ϵ is added to the transfer function $W_1(s)V(s)$ to allow for evaluation of the inverse.

Applying balanced model order reduction to the computed controller, a final controller of 12th order is obtained. The dashed lines in Figures 12 and 13 present the sensitivity $S(s)$ and the transfer function $F(s)S(s)$ corresponding to the reduced order controller $F(s)$ evaluated using the reduced 8th order design model $G(s)$. Thus, the closed-loop characteristics correspond well to the design specifications.
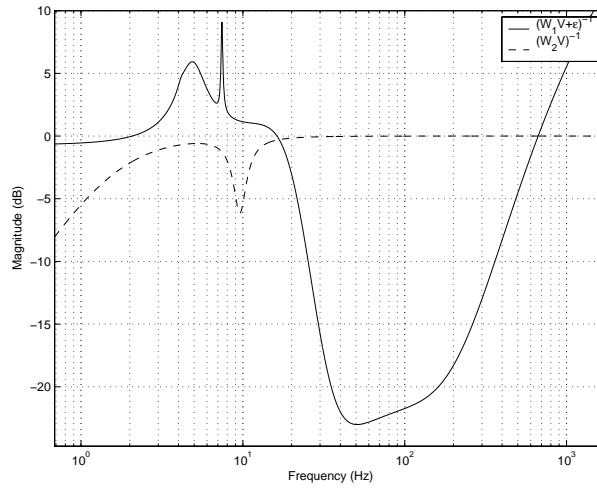
Fig. 11: Magnitudes of the weighting functions $W_1^{-1}(s)V^{-1}(s)$ (solid) and $W_2^{-1}(s)V^{-1}(s)$ (dashed).
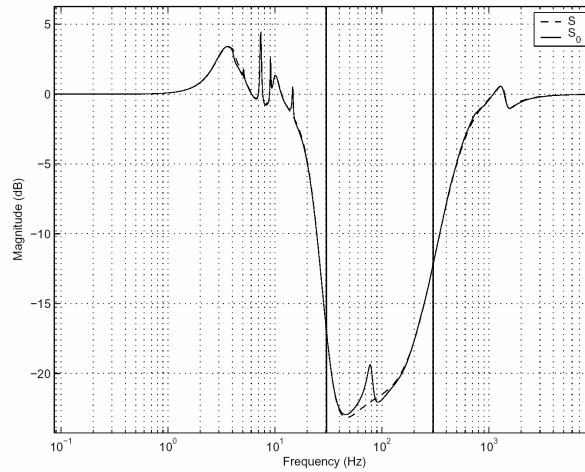

Fig. 12: The sensitivity function $S(s)$ evaluated with the 8th order design model $G(s)$ (dashed) and with the complete 84th order model (solid) using the same 12th order controller. The dominant spectral contents of the engine excitation are assumed to be contained in the frequency region between the two vertical lines.
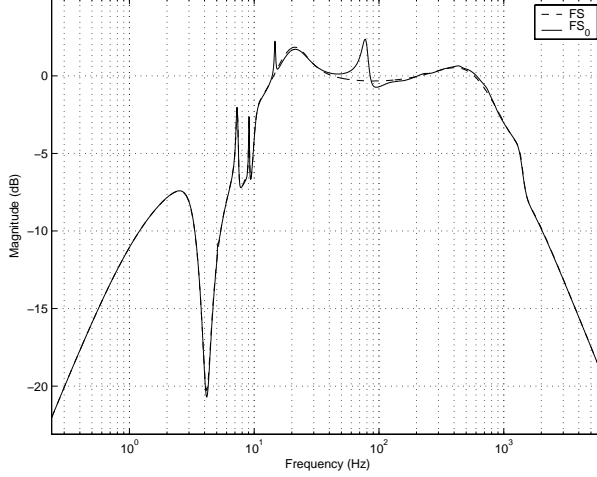
Fig. 13: Magnitude of the transfer function from disturbance to plant input evaluated using the 12th order controller and the 8th order design plant model $G(s)$ (dashed) and the complete 84th order model (solid).

4.2 Performance and Stability

For the closed-loop system to tolerate significant model perturbations, the magnitude of the complementary sensitivity $T(s) = G(s)F(s)S(s)$ has to be kept small (what is considered small will be clear from the discussion below).

Let the true system $G_0(s)$ be related to the design model $G(s)$ according to

$$G_0(s) = (1 + \Delta(s) + \Delta_u(s))G(s) \tag{43}$$

where Δ represents model perturbations due to the missing flexibility and the additional model order reduction from 36 to 8 states. $\Delta_u(s)$ is a representation of all other possible model discrepancies. Then, a necessary and sufficient condition for closed-loop stability (assuming stable perturbation functions $\Delta(s)$ and $\Delta_u(s)$) is

$$\|(\Delta(s) + \Delta_u(s))T(s)\|_\infty < 1 \tag{44}$$

which is fulfilled if

$$|\Delta(s) + \Delta_u(s)| < 1/|T(s)| \tag{45}$$

and, even more conservatively, if

$$|\Delta(s)| + |\Delta_u(s)| < 1/|T(s)| \tag{46}$$

From the transfer function for the 8th order design model $G(s)$, and the transfer function representing the 84th order model, the relative model perturbation $\Delta(s)$ representing errors due to the missing flexibility plus the errors introduced when reducing the 36th order rigid model to an 8th order model, could be determined as $\Delta(s) = 1 - (1 + H_{1D}^{ss}(s))/G(s)$. Here, $H_{1D}^{ss}(s)$ is the transfer function defined by (36). For the controller designed above, it is now possible to estimate the degradation of stability margins and of performance due to the relative modeling errors. Figure 14 shows the maximum allowed magnitude of the relative model perturbation from the nominal design model in percent, i.e. $100/|T(s)|$. Shown in the figure is also the magnitude of the relative error Δ and the remaining margin to relative model errors after subtracting the margin expended by neglecting flexibility and by model order reduction, i.e. $100(1/|T(s)| - |\Delta|)$ in accordance with (46).

As expected from the illustration given in Section 3.4, neglecting the impacts of flexibility on the transfer function corresponds to a rather small relative model error with maximum error approximately equal to 28%. As seen from Fig. 14, this error does not significantly alter the excellent stability margins for this design.

It is also important to consider the effects on achievable performance with respect to model perturbations. Denote with $S_0(s)$ the sensitivity for the true system. The output z_0 of the true plant $G_0(s)$ due to the output disturbance w and the measurement noise n is given by
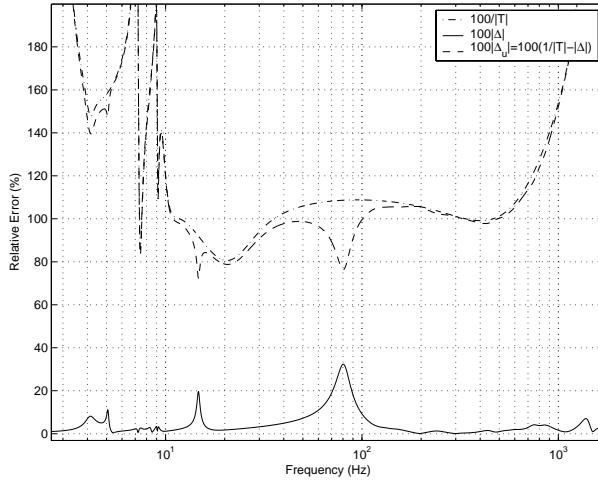
$$z = S_0(s)w - T_0(s)n$$

15

Fig. 14: The upper bound on relative model perturbations for closed-loop stability evaluated using the 8th order design model $G(s)$ (dash dotted), and on model perturbations taking the errors between the 8th order model and the flexible full 84th order model into account (dashed). Shown is also the relative error between the 8th and 84th order models (solid).

Using (43), it could be seen that the plant output z, assuming no perturbations from the design model $G(s)$, is related to the the true output z_0 as

$$\delta z = -S_0(\Delta_u + \Delta)G(s)F(s) \tag{47}$$

where the relative output error $\delta z = (z_0 - z)/z$. Thus, the degradation of performance due to a model perturbation is minor where the sensitivity is low. Figure 12 shows the degradation of performance in terms of achievable sensitivity taking the model errors introduced through neglecting flexibility and performing model order reduction. Due to (47), the degradation is insignificant even at the maximum error of 28%.

5 Conclusions

Active vibration isolation from an arbitrarily, structurally complex receiver is considered. It is shown that when the contribution to the total transmitted force from either a rigid body, local flexible, or global flexible eigenmode is small compared to the actuator force, it does not significantly contribute to the open-loop transfer function. The factors determining the contribution from an individual mode are given where the mode direction relative to the actuator force direction is emphasised as a key factor. It is stressed that minor modal transfer function contribution has the physical interpretation of negligible passive stage force in the direction of the actuator compared to the actuator force. In this context, the relation between model order reduction based on modal and on balanced truncation is investigated. It is shown that for lowly damped systems with certain characteristics, the results when using balanced reduction techniques could potentially be very poor. In addition, the upper bound on the model perturbation due to state truncation is potentially very conservative in this case.

An automotive active vibration isolation problem is used to illustrate the analysis. With reference to the analysis of the influences of flexibility on the open-loop transfer function, it has been shown how to obtain a low order robust controller using a rigid bodies design model. The consequences on performance and stability of neglecting flexibility in the controller design phase are investigated representing the introduced error as a relative output multiplicative model perturbation. For the design of a controller for isolation of the engine vibrations from a flexible subframe, stability and performance are insignificantly affected by the introduced model errors.

The special form of mixed sensitivity optimisation involving three frequency dependent weighting functions for shaping the sensitivity and the transfer function from output disturbance to plant input is utilised for controller design. It is demonstrated how to avoid unwanted pole/zero cancellations of some of the open loop poles. Except for increasing the robustness to parametric uncertainties, this is found to considerably improve the closed-loop characteristics.

6   Acknowledgment

Appendix A: Eigenmode Data

The transfer function given in Eq.(35) corresponding to a complex pole λ_r could be expressed equivalently as in Eq. (48) where the undamped natural frequencies are $\hat{\omega}_{0r} = \sqrt{(\mathrm{Re}(\lambda_r))^2 + (\mathrm{Im}(\lambda_r))^2}$. The damping coefficients are given by $\hat{\epsilon}_r = \mathrm{Re}(\lambda_r)/\sqrt{(\mathrm{Re}(\lambda_r))^2 + (\mathrm{Im}(\lambda_r))^2}$ which means that the damped natural frequencies are $\mathrm{Im}(\lambda_r) = \hat{\omega}_{0r}\sqrt{1 - \epsilon_r^2}$ and $\epsilon_r = 1$ if λ_r are real. The terms in the expression (11) where light damping is assumed answers to the corresponding terms in Eq. (48) if $\hat{\omega}_{0r}$ is well approximated by $\mathrm{Im}(\lambda_r)$, i.e. if the modal damping coefficient is much closer to zero than to one. Table 1 presents the eigenmode data corresponding to the system shown in Fig. 1 including a characterisation of the individual mode shapes.

$$h_r^{ss}(i\omega) = -(k + i\omega c)\frac{(\hat{x}_{(r)}^T q)^2}{\hat{\mu}_r}\frac{1}{(\hat{\omega}_{0r}^2 - \omega^2 + 2i\hat{\epsilon}_r\omega\hat{\omega}_{0r})} \tag{48}$$

References

[1] Fuller C. R., Elliott S. J., and Nelson P. A. *Active Control of Vibration*. ACADEMIC PRESS, 1997.

[2] Spanos J., Rahman Z., and von Flotow A. Active vibration isolation on an experimental flexible structure. In *Proceedings of the SPIE North American Conference on Smart Structures and Intelligent Systems, Albuquerque, New Mexico, SPIE*, volume 1917, pages 674–680, 1993.

[3] Watters B. G., Coleman R. B., Duckworth G. L., and Bukman E. F. A perspective on an active machinery isolation. In *Proceedings of the 27th Conference on Decision and Control, Austin, Texas*, pages 2033–2038, 1988.

[4] Kaplow C. E. Active local vibration isolation applied to a flexible space telescope. *JOURNAL OF GUIDANCE AND CONTROL*, 3(3), 1980.

[5] Blackwood G. H. *Active Vibration Isolation for Controlled Flexible Structures*. Ph.D. Thesis, Department of Aeronautics and Astronautics, Massachusetts Institute of Technology, 1993.

[6] Blackwood G. H. and von Flotow A. H. Active control for vibration isloation despite resonant base dynamics. *DSC-Vol. 38, Active Control of Noise and Vibration*, 1992.

[7] Preumont A., François F., Bossens F., and Abu-Hanieh A. Force feedback versus acceleration feedback in active vibration isolation. *Journal of Sound and Vibration*, 257(4):605–613, 2002.

[8] Kwakernaak H. Robust control and $\mathcal{H}_\infty$-optimization-tutorial paper. *Automatica*, 29(2):225–273, 1993.

[9] MSC.ADAMS. A registered trademark of MSC.Software Corporation.,2 MacArthur Place, Santa Ana, CA 92707, USA.

[10] Gérardin M. and Rixen D. *Mechanical Vibrations, Theory and Application to Structural Dynamics, Second Edition*. JOHN WILEY & SONS, 1998.

[11] Olsson C. *Active Engine Vibration Isolation using Feedback Control*. Tekn. Lic. Thesis ISBN = 91-7373-398-9, Division of Automatic Control, Linköping University, Linköping, Sweden, 2002.

[12] Gawronski W. K. *Dynamics and Control of Structures - A Modal Approach*. Springer-Verlag New York, Inc., 1998.

[13] Zhou K., Doyle J. C., and Glover K. *Robust and Optimal Control*. Prentice Hall, 1996.

[14] Sohoni V. N. and Whitesell J. Automatic linearisation of constrained dynamical models. *Transactoins of the ASME, Vol. 108*, September 1986.

[15] Sefton J. and Glover K. Pole/zero cancellations in the general $\mathcal{H}_\infty$ problem with a reference to a two block design. *Systems & Control Letters*, (14):295–306, 1990.

ID	$\hat{\omega}_{0r}/(2\pi)$ (Hz)	$\mathrm{Re}(\lambda_r)/(2\pi)$ (Hz)	$\mathrm{Im}(\lambda_r)/(2\pi)$ (Hz)	$100\hat{\epsilon}_r$ (%)	$\lvert\hat{x}_r^T q/\hat{\mu}_r\rvert$ $(\mathrm{kgm})^{-1}$	CHARACTER
1	-	-243.2	0.0	1.0	-	(TR;RB)
2	-	-8546.6	0.0	1.0	-	(TR;RB)
3	4.1	-0.2	±4.1	6.0	1.5	(E;RB)
4	5.1	-0.1	±5.1	1.2	0.1	(E;RB)
5	7.4	-0.2	±7.4	2.6	0.8	(E;RB)
6	8.4	-0.1	±8.4	1.7	0.1	(E;RB)
7	9.1	-0.1	±9.1	1.4	0.5	(E;RB)
8	14.7	-0.3	±14.7	1.7	0.5	(E;RB)
9	178.8	-168.6	±59.4	94.3	15.7	(TR;RB)
10	80.0	-7.1	±79.7	8.8	7.2	(SF;RB),(SF;GF)
11	80.6	-6.2	±80.3	7.8	3.0	(SF;RB),(SF;GF)
12	86.9	-7.0	±86.6	8.0	0.1	(SF;RB)
13	118.1	-12.5	±117.4	10.6	1.2	(SF;RB)
14	128.6	-14.2	±127.8	11.0	2.2	(SF;RB)
15	147.8	-17.7	±146.7	11.9	2.8	(SF;RB)
16	229.8	-28.9	±227.9	12.6	1.2	(SF;GF)
17	242.4	-28.5	±240.7	11.7	5.8	(SF;GF)
18	342.8	-126.8	±318.5	37.0	0.3	(TR;RB)
19	337.9	-33.1	±336.3	9.8	3.1	(SF;GF)
20	370.6	-21.1	±370.0	5.7	1.0	(SF;GF)
21	379.5	-57.3	±375.1	15.1	1.4	(SF;LF)
22	379.2	-22.6	±378.5	5.9	0.9	(SF;LF)
23	385.4	-23.6	±384.7	6.1	0.3	(SF;LF)
24	430.4	-130.2	±410.2	30.2	2.2	(SF;LF)
25	449.0	-34.5	±447.7	7.7	5.8	(SF;LF)
26	501.8	-114.4	±488.6	22.8	2.1	(SF;LF)
27	522.0	-57.0	±518.9	10.9	6.9	(SF;LF)
28	531.8	-35.8	±530.6	6.7	1.2	(SF;LF)
29	556.4	-34.7	±555.3	6.2	2.6	(SF;LF)
30	567.8	-116.8	±555.7	20.6	5.7	(SF;LF)
31	577.9	-35.3	±576.8	6.1	2.3	(SF;LF)
32	611.5	-38.1	±610.4	6.2	4.4	(SF;LF)
33	629.5	-35.9	±628.5	5.7	3.1	(SF;LF)
34	666.1	-95.3	±659.3	14.3	6.7	(SF;LF)
35	692.7	-56.3	±690.4	8.1	6.5	(SF;LF)
36	704.4	-101.8	±697.0	14.5	17.4	(SF;LF)
37	753.4	-62.3	±750.8	8.3	8.4	(SF;LF)
38	833.6	-65.0	±831.1	7.8	3.4	(SF;LF)
39	846.7	-81.5	±842.7	9.6	10.9	(SF;LF)
40	874.3	-61.5	±872.1	7.0	5.8	(SF;LF)
41	1420.7	-163.7	±1411.3	11.5	67.4	(TR;RB)
42	1914.8	-181.1	±1906.2	9.5	2.9	(TR;RB)
43	1916.6	-180.7	±1908.0	9.4	0.2	(TR;RB)

Table 1: Eigenmodes data corresponding to the system shown in Fig. 1, sorted on the damped natural frequencies $\mathrm{Im}(\lambda_r)$. Here, E=engine, TR=torque-rod, SF=subframe, RB=rigid body, GF=global flexible, and LF=local flexible.

Figure and Table Captions

Fig. 1: A model of a passenger car engine and subframe suspension system including engine and gear box, subframe, torque-rod, six rubber bushings, and two engine mounts.

Fig. 2: RHS mount static translational stiffness characteristics, in x-,y-, and z-direction.

Fig. 3: Transfer functions from F_s (see Fig. 1) to total force transmitted to subframe in the longitudinal direction of the torque-rod (solid), and to subframe acceleration of the actuator attachment point in the direction of the actuator (dashed).

Fig. 4: Difference between the open-loop transfer functions when modelling the subframe as rigid or as consisting of 24 flexible modes, for force and acceleration measurements respectively.

Fig. 5: Gains of the true system given by Eq. (26) (solid), of the system reduced using modal truncation (dashed), and of the system reduced by balanced truncation of the states corresponding to the two smallest HSVs γ_3 and γ_4 in Eq. (30) (dash-dotted).

Fig. 6: Gains of the true system given by Eq. (26) (solid), of the system reduced using modal truncation (dashed), and of the system reduced by balanced truncation of the states corresponding to the HSVs γ_2 and γ_3 in Eq. (30) (dash-dotted).

Fig. 7: Magnitudes of three transfer functions; $|H_{1D}^{ss}(i\omega)|$ (solid), $|1 + H_{\Sigma 1}(i\omega)|$ as defined by (37) (dashed), and $|H_{\Sigma 2}(i\omega)| = |H_{1D}^{ss}(i\omega) - H_{\Sigma 1}(i\omega)|$ (dash dotted).

Fig. 8: Magnitudes of three transfer functions; $|H_{1D}(i\omega)|$ (solid), $|H_{\Sigma 1}(i\omega)|$ defined by (37) (dashed), and $|G_D(i\omega)|$ (dash dotted)..

Fig. 9: Magnitudes corresponding to $|h_{10}^{ss}|$ (solid), $|h_{11}^{ss}|$ (dashed), and $|h_{12}^{ss}|$ (dash dotted).

Fig. 10: Some high frequency poles and zeros of the system shown in Fig. 1 corresponding to the two transfer functions presented in Fig. 3, i.e. from actuator force to total transmitted force and receiver acceleration respectively.

Fig. 11: Magnitudes of the weighting functions $W_1^{-1}(s)V^{-1}(s)$ (solid) and $W_2^{-1}(s)V^{-1}(s)$ (dashed).

Fig. 12: The sensitivity function $S(s)$ evaluated with the 8th order design model $G(s)$ (dashed) and with the complete 84th order model (solid) using the same 12th order controller. The dominant spectral contents of the engine excitation are assumed to be contained in the frequency region between the two vertical lines.

Fig. 13: Magnitude of the transfer function from disturbance to plant input evaluated using the 12th order controller and the 8th order design plant model $G(s)$ (dashed) and the complete 84th order model (solid).

Fig. 14: The upper bound on relative model perturbations for closed-loop stability evaluated using the 8th order design model $G(s)$ (dash dotted), and on model perturbations taking the errors between the 8th order model and the flexible full 84th order model into account (dashed). Shown is also the relative error between the 8th and 84th order models (solid).

Table 1: Eigenmodes data corresponding to the system shown in Fig. 1, sorted on the damped natural frequencies $\text{Im}(\lambda_r)$. Here, E=engine, TR=torque-rod, SF=subframe, RB=rigid body, GF=global flexible, and LF=local flexible.)